ACS APPLIED MATERIALS & INTERFACES

RESEARCH ARTICLE

www.acsami.org

Liquid Water Transport in Polylactide Homo and Graft Copolymers

Eric M. Davis,[†] Grayce Theryo,[‡] Marc A. Hillmyer,[‡] Richard A. Cairncross,[†] and Yossef A. Elabd*[,†]

[†]Department of Chemical and Biological Engineering, Drexel University, Philadelphia, Pennsylvania 19104, United States

[‡]Department of Chemistry, University of Minnesota, Minneapolis, Minnesota 55455, United States

Supporting Information

ABSTRACT: The successful design of new biodegradable, renewable resource plastics as replacements to commodity barrier plastics would benefit from an accurate measurement of sorption and diffusion of liquids. In this study, the diffusion of liquid water in amorphous polylactide [PLA] and a PLA graft copolymer, poly(1,5-cyclooctadiene-*co*-5-norbornene-2-methanol-*graft*-DL-lactide) [PCNL], was examined with time-resolved Fourier transform infrared attenuated total reflectance (FTIR-ATR) spectroscopy. Non-Fickian behavior was observed for all experiments, indicated by a slow approach to steady state due to diffusion and polymer relaxation occurring on similar time scales. This non-Fickian behavior highlights the variability of the sorption isotherms reported in the literature, where others have collected nonequilibrium sorption behavior (instead of true steady-state equilibrium sorption) at different time points and film thicknesses. The dynamic infrared data provided direct evidence for both water diffusion and water-induced polymer relaxation, where both were quantified and regressed to a diffusion-relaxation model to determine the diffusion coefficient and the polymer relaxation time constant. In addition to the successful measurement and modeling of the diffusion-relaxation phenomena for diffusion of a liquid in a nonequilibrium state glassy polymer, this study also determined that the diffusivity of water in the PLA graft copolymer (with only 5 wt % rubber) was 3-fold lower than in the PLA homopolymer.

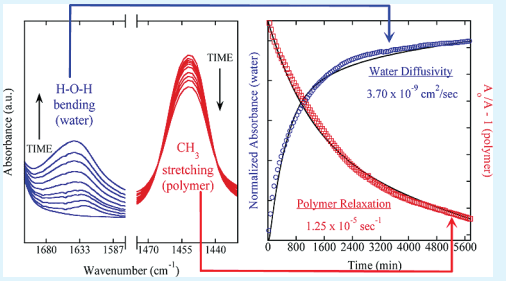

KEYWORDS: polymer, sustainable, green, water, films, membranes

INTRODUCTION

Polylactide (PLA) is actively being pursued as a sustainable replacement to widely used commodity plastics because it is produced from renewable sources and readily degrades into benign naturally occurring small molecule products.[1−3] For many applications (e.g., medical implants, packaging), an accurate assessment and fundamental understanding of water sorption and diffusion in PLA is of great interest. Previous investigations report low water solubilities in PLA (e.g., < 1 wt % at vapor activities >0.8);[4] however, there are only a few reports on water vapor sorption and diffusion in PLA and the values reported vary among these studies.[4−7] Furthermore, there are even fewer reports on the sorption and diffusion of liquid water in PLA,[8] which is particularly relevant for applications such as plastic water bottles and coated drug eluting stents.[1,2]

Typically, sorption measurements of liquids in polymers consist of immersing a free-standing polymer film in the liquid, manually removing the sample from the liquid, blotting the surface free of surface liquid, quickly weighing the sample on a balance, and then reimmersing the film in the liquid. This process is repeated many times over a short time interval to collect early time kinetic data to measure diffusion, whereas the long time steady-state value of the total amount of water taken up by the film is reported as equilibrium sorption. This ex situ technique introduces significant error when attempting to collect many data points over a short time frame. Therefore, a more sensitive and accurate technique that can measure liquid water sorption and diffusion in PLA is highly desirable.

Recently, time-resolved Fourier transform infrared attenuated total reflection (FTIR-ATR) spectroscopy has been used with increasing frequency to examine the diffusion of small molecules in polymers.[9] Specifically, time-resolved FTIR-ATR spectroscopy is a noninvasive, in situ technique that can provide accurate, reliable short-time data for the diffusion of liquids in polymers. In this technique, the entire mid-infrared spectrum of both the diffusant(s) and the polymer are measured as a function of time, providing highly sensitive molecular-level contrast between the two. In addition to uncovering molecular changes in the diffusant/polymer system (e.g., multicomponent diffusion, polymer relaxation),[10−12] FTIR-ATR can also be used to quantify molecular interactions between the diffusant and the polymer.[13]

Theryo et al.[14] recently reported on the synthesis of a new PLA graft copolymer, poly(1,5-cyclooctadiene-*co*-5-norbornene-2-methanol-*graft*-DL-lactide) [PCNL], with significantly enhanced toughness compared to that of the PLA homopolymer. The graft copolymer contains 5 wt % rubber (as the backbone), which results in a phase-segregated polymer with nanoscopic dispersed rubber domains, evidenced by electron microscopy and X-ray

Received: July 1, 2011
Accepted: September 2, 2011
Published: September 02, 2011

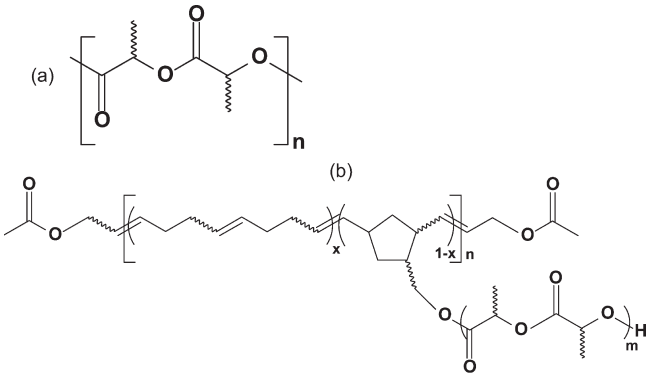

Figure 1. (a) Polylactide [PLA] and (b) PLA graft copolymer [PCNL].

scattering. In addition to mechanical property measurements, an accurate assessment of barrier properties when the material is in contact with liquid water is of interest. In addition to the work by Theryo et al.,[14] others have attempted to improve the barrier properties of PLA with strategies such as surface treatments or the addition of impermeable fillers.[15−19] However, without an accurate measurement of the diffusion and sorption of liquids in PLA and its variants, it will be difficult to design new biodegradable plastics with improved barrier properties.

In this work, the diffusion of liquid water in this new PLA graft copolymer[14] and the PLA homopolymer was examined with time-resolved FTIR-ATR spectroscopy, where accurate water sorption kinetics were measured. Non-Fickian behavior was observed for all polymers in this study, which can be ascribed to both water diffusion and water-induced polymer relaxation occurring on similar time scales in a nonequilibrium glassy polymer. Unlike gravimetry,[20] time-resolved FTIR-ATR spectroscopy captures both of these phenomena simultaneously, where a diffusion-relaxation model can determine both the relaxation and diffusion time with minimal fitting parameters. Interestingly, in this study, the diffusivity of water in the PLA graft copolymer was found to be 3-fold lower than in the PLA homopolymer.

EXPERIMENTAL SECTION

Materials. A PLA graft copolymer and PLA homopolymer (50/50 D and L- stereoisomers) were synthesized previously (Figure 1).[14] Briefly, the PLA graft copolymer was synthesized by using ring-opening metathesis polymerization (ROMP) and subsequent ring-opening transesterification polymerization (ROTEP) to yield poly(1,5-cyclooctadiene-*co*-5-norbornene-2-methanol-*graft*-DL-lactide) [PCNL] (see Figure 1b), which consists of a rubbery copolymer (5 wt % of the polymer) with PLA side chains. The number-averaged molecular weights were calculated using ^{1}H NMR spectroscopy and were determined to be 659, 57, and 59 kg/mol for the entire PCNL molecule, each PLA side chains on the graft copolymer, and the PLA homopolymer [PLA control], respectively. For additional comparison, commercially available PLA (PLA 4032D; 1.5% D- stereoisomer)[21] was purchased from Nature Works LLC in pellet form. Chloroform (99.8% purity; ACS reagent) was purchased from Aldrich. Ultrapure reverse osmosis (RO) water (resistivity ~16 MΩ cm) was used for all diffusion and sorption experiments.

Film Preparation. PLA/chloroform solutions were produced for all PLA samples, PCNL, PLA control, and PLA 4032D, by dissolving the appropriate PLA sample in chloroform at 5% w/v and mixing for 24 h to ensure a clear, homogeneous solution. PLA film fabrication consisted of solution casting the PLA/chloroform solution onto a Teflon Petri dish to produce free-standing films for gravimetric experiments (water sorption) or solution casting onto the ATR crystal surface for time-resolved FTIR-ATR spectroscopy experiments (water diffusion). After solution casting onto a given surface for 24 h, the PCNL and PLA control were subsequently annealed at 60 °C under vacuum for 3 h. The PLA 4032D sample was processed differently after solution casting. This procedure entailed annealing the film for 3 h at 60 °C, annealing at 195 °C for an additional 3 h followed by a rapid quench to room temperature, where all steps were continually purged under dry nitrogen (nitrogen passed through a moisture trap (Restek) packed with indicating Drierite and Molecular Sieve 5A). As expected, the PCNL (PLA grafts) and PLA control films were completely amorphous and the PLA 4032D film was almost completely amorphous (ca. 1% crystallinity) as confirmed by differential scanning calorimetry (see the Supporting Information, Figure S1). After film fabrication, all PLA films were immediately stored in a desiccator prior to sorption and diffusion experiments. Immediately following each sorption and diffusion experiment, the thickness of the PLA films was measured using a digital micrometer (Mitutoyo) with a 1 μm accuracy. Each film thickness was an average of five individual measurements at different positions along the length of the film.

Gravimetric Sorption. Free-standing films were submerged in liquid water at room temperature (~25 °C), quickly removed at periodic time intervals, carefully blotted with a low-lint cloth (Kimwipes) to remove excess surface liquid, and immediately weighed (wet weight, $m(t)$). This process was continued until a constant mass was recorded over numerous time intervals (equilibrium wet weight, m_{eq}). Sorption kinetic data were regressed to the analytical solution of the one-dimensional mass continuity equation for planar coordinates with constant mass boundary conditions[22]

$$\frac{m(t) - m_0}{m_{eq} - m_0} = 1 - \frac{8}{\pi^2}\sum_{n=0}^{\infty}\frac{1}{(2n+1)^2}\exp[-D_w f^2 t] \quad (1)$$

$$f = \frac{(2n+1)\pi}{2L} \quad (2)$$

where m_0 and L are the initial polymer weight at $t = 0$ and the polymer film thickness, respectively. D_w is the diffusion coefficient of water in the polymer, which is the only adjustable parameter in the regression. Equilibrium sorption was recorded at equilibrium or steady state as the water uptake normalized by the dry polymer weight (g of water/g of polymer; g_w/g_p). The dry PLA films weighed 300 mg on average. The weights were recorded with an analytical balance (Precisa XR 125SM-FR) with an accuracy of 10 μg.

Time-Resolved FTIR-ATR Spectroscopy. For liquid water transport experiments, time-resolved infrared spectra were collected using an FTIR Spectrometer (Nicolet 6700 Series; Thermo Electron) equipped with a horizontal, temperature-controlled ATR cell (Specac Inc.). The PLA films were cast on a multiple reflection, trapezoidal zinc selenide ATR crystal (Specac Inc.) with 45° beveled faces. All spectra were collected using a liquid nitrogen-cooled mercury−cadmium-telluride (MCT) detector with 32 scans per spectrum at a resolution of 4 cm^{-1}, where a spectrum was collected every 150 s. All transport experiments were conducted at 25 °C, controlled by a temperature jacket (circulating water bath) on the ATR flow through cell.

Before each transport experiment, a background spectrum of the ATR crystal was collected and all subsequent collected spectra were subtracted from this spectrum. Then, a PLA-coated ATR crystal was mounted into the ATR cell with a Kalrez gasket and the cell was sealed. To begin each transport experiment, RO water was transferred by pipet into the ATR cell in the space (V = 550 μL) above the polymer film (the side opposite the polymer-crystal interface) and sealed to prevent water evaporation during the experiment. This was followed by time-resolved infrared spectral collection.

Unsteady-state diffusion of water in PLA films for this ATR configuration[9] can be described by the one-dimensional concentration continuity equation

$$\frac{\partial C}{\partial t} = D_w \frac{\partial^2 C}{\partial z^2} \tag{3}$$

where C is the concentration of the diffusant (in this case water), D_w is the effective concentration-averaged diffusion coefficient of water in the polymer, and t and z are time and space coordinates, respectively. An appropriate set of initial and boundary conditions for the ATR experiment are[9]

$$C = C_0 \text{ at } 0 < z < L \text{ and } t = 0 \tag{4}$$

$$\frac{dC}{dz} = 0 \text{ at } z = 0 \text{ and } t \geq 0 \tag{5}$$

$$C = C_{eq} \text{ at } z = L \text{ and } t \geq 0 \tag{6}$$

where L is the polymer film thickness, C_0 is the initial concentration (zero for this experiment), and C_{eq} is the final equilibrium concentration of water in the polymer (i.e., constant surface concentration of water in the polymer at the water-polymer interface). The coordinates were chosen so that $z = 0$ is the polymer-crystal interface and $z = L$ is the water-polymer interface.

An analytical solution to eq 3 with these initial and boundary conditions (eqs 4−6) is given as[21]

$$\frac{C(t,z) - C_0}{C_{eq} - C_0} = 1 - \frac{4}{\pi} \sum_{n=0}^{\infty} \frac{(-1)^n}{2n+1} \exp[-D_w f^2 t] \cos[fz] \tag{7}$$

Concentration can be related to the ATR experimental absorbance through the use of the differential form of the Beer−Lambert law (eq 8), where an evanescent wave propagates into the polymer due to total internal reflection at the polymer−crystal interface.

$$A = \int_0^L \varepsilon^* C \exp(-2z/d_p) dz \tag{8}$$

In eq 8, A is the ATR absorbance value, ε^* is the molar extinction coefficient (which can be considered constant under the assumption of weak IR absorbance, which is the case in this study), and d_p is the depth of penetration for the IR radiation in the polymer

$$d_p = \frac{\lambda}{2\pi n_1 \sqrt{\sin^2 \theta - (n_2/n_1)^2}} \tag{9}$$

where n_1 and n_2 are the refractive indices of the ATR crystal and polymer, respectively, θ is the angle of incidence, and λ is the wavelength of absorbed light. The depth of penetration is essentially the sampling distance into the polymer, which is when the evanescent wave has decayed to approximately 1/3 of its maximum intensity (~1 μm for these experiments). Substituting eq 7 into eq 8 and integrating results in the following expression

$$\frac{A(t) - A_0}{A_{eq} - A_0} = 1 - \frac{(8/d_p)}{\pi[1 - \exp(-2L/d_p)]} \sum_{n=0}^{\infty} \frac{1}{2n+1} \times \left(\frac{\exp(-D_w f^2 t)[f \exp(-2L/d_p) + (-1)^n (2/d_p)]}{((2/d_p)^2 + f^2)} \right) \tag{10}$$

where $A(t)$, A_0, and A_{eq} are the ATR absorbance at time t, at initial time, and at equilibrium (i.e., long times), respectively.

When $L/d_p > 10$, the concentration profile near the polymer−crystal interface is constant resulting in a location-specific solution (thick-film approximation).[11]

$$\frac{A(t, z \to 0) - A_0}{A_{eq} - A_0} = 1 - \frac{4}{\pi} \sum_{n=0}^{\infty} \frac{(-1)^n}{2n+1} \exp[-D_w f^2 t] \tag{11}$$

In other words, the concentration profile or gradient in the measured region (~1 μm in the polymer film near the polymer/crystal interface) is constant when the polymer film thickness is much larger than the sampling depth, resulting in a location-specific measurement. Therefore, water is imposed on one side of the film and measured on the other side as a function of time. This differs from the gravimetric experiment described above, where that technique is measuring a weight gain averaged over the entire thickness of the film. The experimental time-resolved ATR absorbance of water in PLA can therefore be regressed to eq 11 to determine an effective diffusion coefficient, where this variable is the only adjustable parameter in the model. More details regarding the apparatus and experimental procedures can be found elsewhere.[9,11,23]

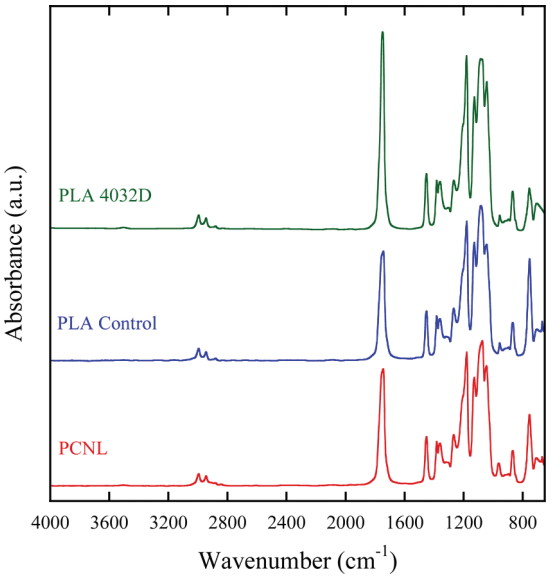

Figure 2. Infrared spectra of dry PCNL, PLA control, and PLA 4032D. Spectra are offset for clarity.

RESULTS AND DISCUSSION

The infrared spectra of PCNL, PLA control, and PLA 4032D are shown in Figure 2 prior to exposure to water. All three spectra are nearly identical and contain all of the key infrared bands associated with amorphous PLA (see Table 1). It is important to note that several bands shift and additional bands appear when PLA is semicrystalline.[24−26] For example, in semicrystalline PLA, a new band appears at 921 cm^{-1} (the band at 960 cm^{-1} decreases), the band at 1747 cm^{-1} shifts to 1760 cm^{-1}, and the band at 1452 cm^{-1} splits into two bands at 1457 and 1442 cm^{-1}. No bands associated with crystallinity were observed in this study, which corroborate the thermal analysis data (see the Supporting Information, Figure S1). It is also interesting to note that the infrared spectrum for PCNL was not that different than the other PLA samples. This may be due to the fact that most of the chemical bonds in PCNL are similar to those in PLA and the other chemical bonds in PCNL that are not in PLA (e.g., CH_2) are weak absorbers to the infrared.

Figure 3 shows the time-resolved infrared spectra of liquid water diffusing in a PCNL film. The inset in Figure 3 highlights

Table 1. Infrared Band Locations for Amorphous PLA

bond vibrations	band location (cm^{-1})	ref
δ(OH)	3503	27
δ_{as}(CH)	2995	26,28−30
δ_{as}(CH)	2944	26−29
δ(C═O)	1747	23−29,31−35
δ_{as}(CH_3)	1452	24−26,28,29,31,33,36
δ_s(CH_3)	1381	24,26,29,31
δ(CH) + δ_s(CH_3)	1363	24,26,29,31
δ(CH)	1317	29,31
δ(CH) + ν(COC)	1268	23−25,30,31,35,37
ν_{as}(COC)	1182	23−26,30−32,35
r_{as}(CH_3)	1128	23,24,29,31−33
ν_s(COC)	1081	23−25,29,31
ν(C − CH_3)	1047	23,24,29,31−33
ν(C − C) + r(CH_3)	960, 865	24−26,29−31,36,38
δ(C═O)	751	29
γ(C═O)	705	29

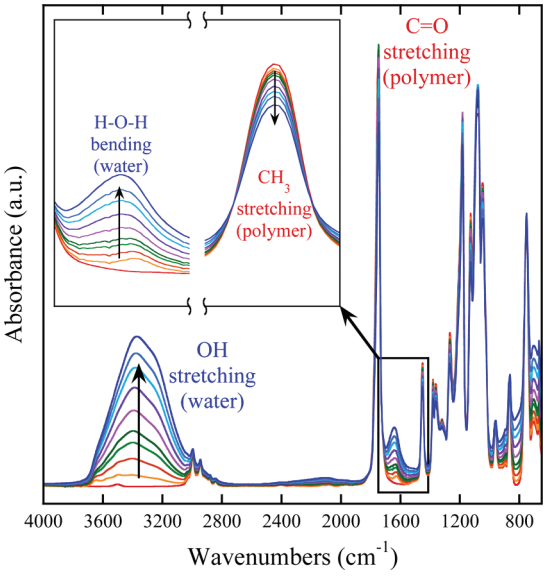

Figure 3. Infrared spectra of liquid water diffusing into dry PCNL at 25 °C at selected time intervals. The inset shows the increase of the H−O−H bending band (water) and the decrease of the CH_3 stretching band (polymer) with time. Arrows indicate the direction of spectral change with time.

two bands of interest for this study, where the intensity of the H−O−H bending of water (1641 cm^{-1}) increases with time, representing the diffusion of water in PCNL, and the intensity of the CH_3 stretching of the polymer (1452 cm^{-1}) decreases with time, representing the water-induced relaxation of the polymer.

Figure 4 shows the normalized (to their final value) integrated absorbance of these two bands as a function of time. The solid line represents the regression of the water diffusion data to the solution of the Fickian diffusion model (eq 11), where the diffusion coefficient, D_w, was the only adjustable fitting parameter. It is clear from this regression that the diffusion of liquid

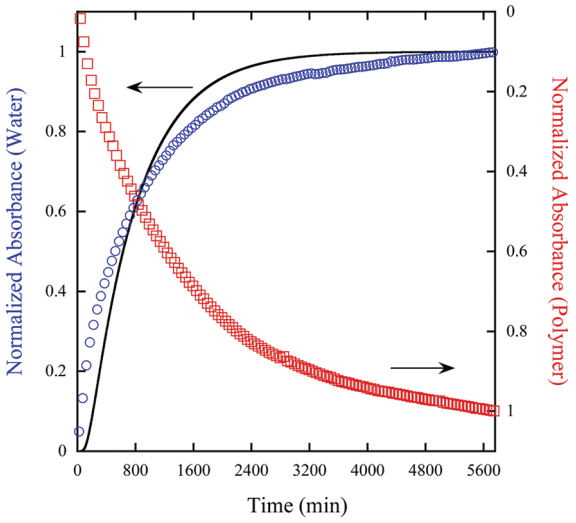

Figure 4. Normalized, integrated absorbance of the H−O−H bending of water (blue circles) and the CH_3 stretching of PCNL (red squares) as a function of time at 25 °C. The line represents a regression to the Fickian model (eq 11).

water in PCNL cannot be adequately described by Fickian diffusion. Similar results were also observed for liquid water diffusion in the PLA control and the PLA 4032D.

Other investigations on the diffusion of small molecules in glassy polymers have yielded non-Fickian or anomalous sorption kinetic profiles (collected with gravimetric apparatus) that appear similar to the ATR water diffusion data in Figure 4.[20] This behavior has been attributed to diffusion and polymer relaxation occurring on similar time scales in a nonequilibrium system (glassy polymer), where diffusion is driven by the concentration gradient of the diffusant and polymer relaxation is a response to the stress imposed by the diffusant.[20,39,40] Unlike gravimetric sorption, the data from time-resolved FTIR-ATR spectroscopy captures both of these phenomena simultaneously (Figure 4), confirming this diffusion-relaxation hypothesis.

Therefore, with the ability to measure both diffusion and relaxation within the same experiment, a model can be developed that incorporates both of these phenomena. Other investigators have developed a model that incorporate both phenomena, but the implementation of this model results in regressing one set of data (water sorption kinetics) to a model with six fitting parameters.[20] In this work, two coupled sets of data can be regressed to a model with minimal fitting parameters. Recently, Hallinan et al.[12] observed similar diffusion−relaxation results for water vapor diffusion in Nafion using the same technique as in this study. They developed a coupled diffusion−relaxation model to regress both sets of experimental data: water diffusion and polymer relaxation. In this study, the same model, summarized below, was implemented.

First, the polymer relaxation data (polymer absorbance decay with time) can be regressed to a relaxation model to determine a relaxation time constant, which can then be used to regress the water diffusion data (water absorbance increase with time) to a diffusion-relaxation model to determine the diffusion coefficient. The model regresses two sets of data to two equations. For the polymer relaxation component, a three-element viscoelastic model was chosen, consisting of a one-element viscous dashpot in series with a two-element Kelvin (or Voigt) model (a viscous

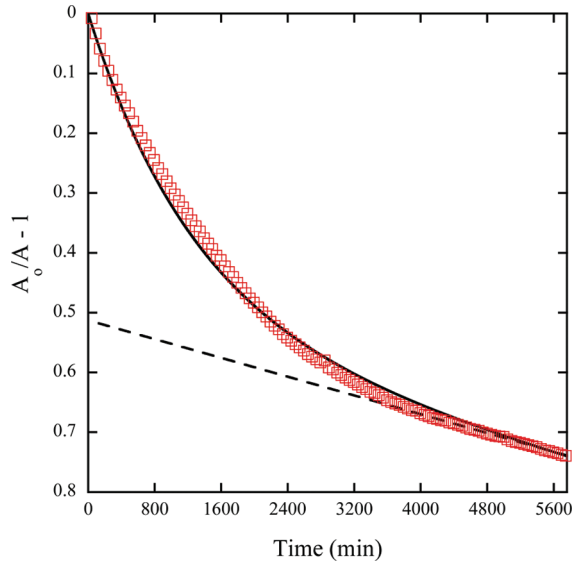

Figure 5. Regression of the time-resolved PCNL CH_3 stretching infrared absorbance data (red squares) to the polymer relaxation model (25 °C). The dashed and solid lines represent the late-time linear solution and full solution of eq 14, respectively, where the relaxation time constant, β, was the only fitting parameter for the full regression.

dashpot in parallel with an elastic spring).

$$\varepsilon = \frac{\sigma}{\eta}t + \frac{\sigma}{E}(1 - \exp(-\beta t)) \tag{12}$$

In eq 12, σ, ε, η, E, and β are the stress, strain, dynamic viscosity, Young's modulus, and relaxation time constant, respectively. In this model, the stress, viscosity, and modulus are all assumed to be constant due to the low solubility of water in PLA. The polymer strain can be related to the infrared absorbance data with the use of the Beer−Lambert law

$$\varepsilon = \frac{\Delta V}{V_0} \approx \frac{1/C - 1/C_0}{1/C_0} \approx \frac{1/A - 1/A_0}{1/A_0} = \frac{A_0}{A} - 1 \tag{13}$$

where V_0, C_0, and A_0 are the initial volume, concentration, and absorbance, respectively. Therefore, the measured polymer absorbance can be considered inversely proportional to the strain or water-induced swelling of the polymer. Physically, this is the result of water inducing stress on the polymer during diffusion, which results in a polymer strain response or increase in polymer volume in the fixed infrared sampling depth region (evanescent wave). Because absorbance is proportional to concentration, the increase in volume results in a decrease in the polymer absorbance (see Figure 4). Therefore, eq 12 can be rewritten in terms of the experimental infrared absorbance of the polymer CH_3 stretching band with the use of eq 13.

$$\frac{A_0}{A} - 1 = \frac{\sigma}{\eta}t + \frac{\sigma}{E}(1 - \exp(-\beta t)) \tag{14}$$

For time-resolved infrared experimental data, a late-time solution to eq 14 represents only the viscous contribution of the relaxation model as the exponential term approaches zero. This results in a linear equation, where the slope (σ/η) and intercept (σ/E) represent the mechanical constants of the model. Figure 5 shows a regression of the late-time polymer CH_3 stretching absorbance data to the late-time linear solution of eq 14, where $\sigma/\eta = 6.5 \times 10^{-7}$ Pa/(Pa s) and $\sigma/E = 0.51$ Pa/Pa. Using these constants, the entire data set can be regressed to the full relaxation model, eq 14, with the relaxation time constant, β, as the only adjustable fitting parameter of the full regression. This regression is also shown in Figure 5 with a regressed relaxation time of 1.25×10^{-5} s^{-1}. It is clear from Figure 5 that the three-element viscoelastic model chosen agrees well with polymer relaxation data.

With an independent measure of polymer relaxation, the regressed relaxation time constant can now be applied to a regression of the water diffusion data with the use of a diffusion-relaxation model.

$$\frac{A(t) - A_0}{A_{eq} - A_0} = F_A\left[1 - \frac{4}{\pi}\sum_{n=0}^{\infty}\frac{(-1)^n}{2n+1}\exp[-D_w f^2 t]\right] + F_B[w_2 t + w_1(1 - \exp(-\beta t))] \tag{15}$$

$$w_1 = \frac{\frac{\eta}{E}}{t_f + \frac{\eta}{E}} \tag{16}$$

$$w_2 = \frac{1}{t_f + \frac{\eta}{E}} \tag{17}$$

Here, eq 15 is a weighted sum of the Fickian diffusion (eq 11) and the three-element viscoelastic relaxation model (eq 14 normalized by the final strain). In eq 15, F_A and F_B are the weighting fractions of the diffusion and relaxation portions, respectively, and w_1 and w_2 are the dimensionless constants that arise from normalizing eq 14 with respect to strain at long times (t_f) in order to incorporate this into a normalized diffusion-relaxation solution. Therefore, the relaxation portion of eq 15 is now expressed as $(A(t) - A_0)/(A_{eq} - A_0))$ instead of $(A_0/A(t) - 1)$, where the latter was used to regress the polymer relaxation data with the use of eq 14. In order to validate the use of the relaxation time constant determined from the regression using eq 14 into the regression of the water diffusion data using eq 15, the polymer relaxation data expressed as both $(A(t) - A_0)/(A_{eq} - A_0))$ and $(A_0/A(t) - 1)$ were compared. The average percent difference between these two data sets was less than 4% for each experiment conducted in this study. Also, the difference in the regressed constants from the late-time and full regressions of the polymer relaxation data plotted either as $(A(t) - A_0)/(A_{eq} - A_0))$ or $(A_0/A(t) - 1)$ was negligible.

Equation 15 can therefore be applied to the water diffusion data, which has one part that accounts for water sorption due to a concentration gradient and another part that accounts for the additional water sorption due to nonequilibrium water-induced relaxation. Similar to the polymer relaxation model (eq 14), there is a late-time solution of the diffusion−relaxation model (eq 15) that represents only the viscous loss due to polymer relaxation, where both the exponential terms in the diffusion and elastic relaxation portions of the model approach zero at late times. Figure 6 shows the regression of the late-time water diffusion data (time-resolved H−O−H water bending infrared absorbance) to the late-time linear solution of eq 15, where the regressed slope $(F_B w_2)$ and intercept $(F_A + F_B w_1)$ are 3.73×10^{-7} s^{-1} and 0.87, respectively. Using the regressed constants $(\sigma/\eta = 6.5 \times 10^{-7}$ Pa/(Pa s), $\sigma/E = 0.51$ Pa/Pa) from the late-time regression of the polymer relaxation data (Figure 5), the weighting fractions for diffusion (F_A) and relaxation (F_B) were determined to be

0.56 and 0.44, respectively. Note that the same time interval in both Figures 5 and 6 were used for the linear late-time regression, where the entire linear portion of Figure 5 was used in late-time regression. Now, with known values of σ/η, σ/E, F_A, F_B, and β, the entire water diffusion data set can be regressed to the full diffusion-relaxation model (eq 15) with the diffusion coefficient of water, D_w, as the only adjustable parameter of the full regression. Figure 6 shows this full regression with a water diffusion coefficient of 3.70×10^{-9} cm^2/s.

The diffusion−relaxation model approach was also applied to water diffusion in the PLA control and PLA 4032D. The regressions are shown in Figures 7 and 8 and the results from this analysis are listed in Table 2 for each experiment.

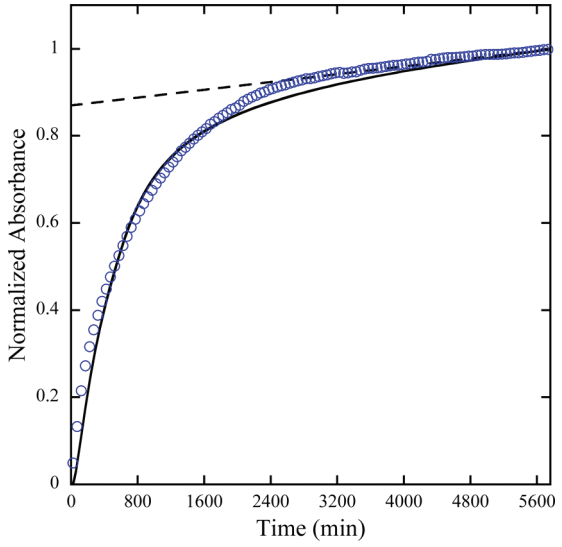

Figure 6. Regression of the time-resolved water H−O−H bending infrared absorbance data (blue circles) to the diffusion-relaxation model (25 °C) for PCNL. The dashed and solid lines represent the late-time linear solution and full solution of eq 15, respectively, where the diffusion coefficient of water, D_w, was the only fitting parameter for the full regression.

With the diffusion coefficient and relaxation time constant determined from the diffusion-relaxation model, a diffusion time ($\tau_D \approx L^2/D$) and a relaxation time ($\tau_R \approx 1/\beta$) can be calculated. A ratio of these times is referred to as the diffusion Deborah (De) number.[41] Table 2 shows that all of the De numbers for each experiment in this study are on the order of 1, which is indicative of when diffusion and relaxation occur on similar time scales, confirming the observed anomalous dynamics. Also, the diffusion and relaxation portions appear to be approximately equally weighted in all experiments (shown by the value of F_A in Table 2). It is important to highlight that the diffusivities of water in PLA control and PLA 4032D are similar, which was expected, but the diffusivity of water in PCNL was 3 times lower.

This result was unexpected based on simple calculations using models for diffusion in heterogeneous polymers developed by many other investigators, where the effective diffusivity scales with volume fraction of the two phase segregated domains.[38] Previous work by Theryo et al.[14] shows a phase segregated morphology for PCNL, where dispersed PCN domains (5 wt %) of ∼10−30 nm were observed with electron microscopy and morphology and spacing were confirmed with small-angle X-ray scattering. Assuming the PCN were impermeable domains, then one would calculate only a small reduction in diffusivity due to the low PCN volume fraction. However, PCN should have a diffusivity similar to or even higher than PLA as rubber polymers typically have higher diffusivities than glassy polymers. Therefore, the measured effective diffusivity should be similar or even higher than PLA.

To examine this more closely, Figure 9 shows a comparison of the rate of water sorption for the PCNL (film thickness of 134 μm) to PLA 4032D at similar film thicknesses. As expected, the rate of water sorption in PLA 4032D is faster than PCNL. In other words, if the diffusivity of the PLA graft copolymer were similar to the homopolymer, the rate of sorption would also be similar. These results confirm the lower calculated diffusivity for the PCNL from the diffusion-relaxation model. Additionally, a plot of the polymer absorbance (strain response) to that of the water absorbance (water diffusion) provides additional information regarding the time scale on which both phenomena occur.

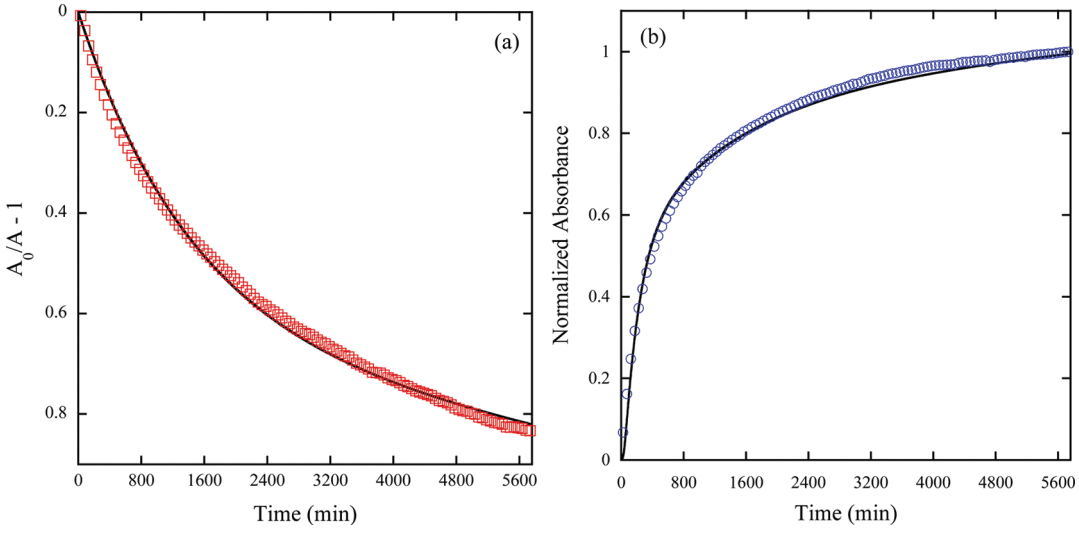

Figure 7. PLA control (25 °C): (a) water-induced polymer relaxation: time-resolved polymer CH_3 stretching infrared absorbance data (red squares) and (b) water diffusion: time-resolved water H−O−H bending infrared absorbance data (blue circles). The solid lines represent a regression to the polymer relaxation model, eq 14, and the diffusion-relaxation model, eq 15, respectively.

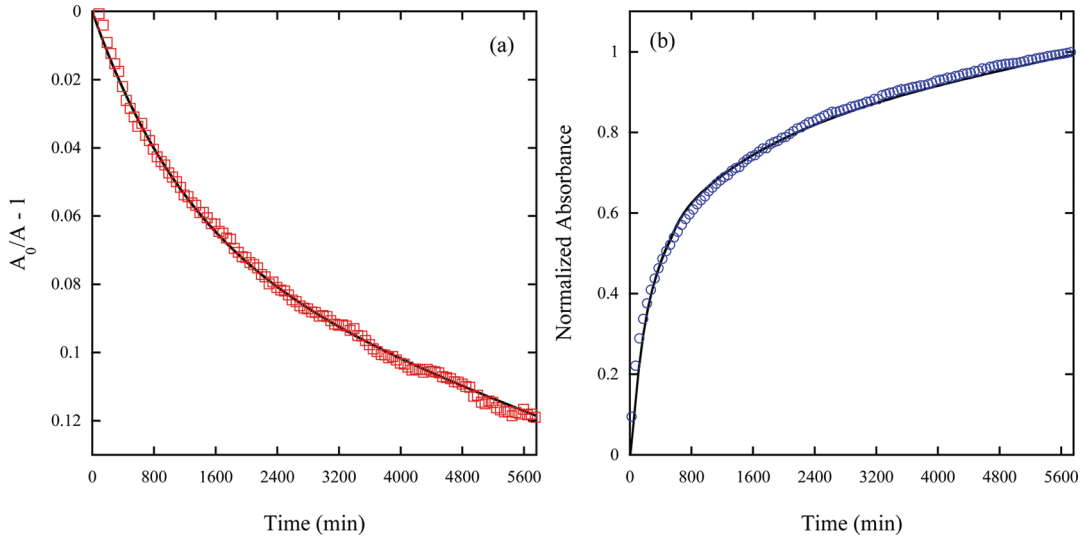

Figure 8. PLA 4032D (25 °C): (a) water-induced polymer relaxation: time-resolved polymer CH_3 stretching infrared absorbance data (red squares) and (b) water diffusion: time-resolved water H−O−H bending infrared absorbance data (blue circles). The solid lines represent a regression to the polymer relaxation model, eq 14, and the diffusion-relaxation model, eq 15, respectively.

Table 2. Diffusion−Relaxation Model Results for PCNL, PLA Control, and PLA 4032D

sample	L (μm)	$\beta \times 10^5$ (s^{-1})	$D_w \times 10^8$ (cm^2/s)	F_A	τ_R (min)	τ_D (min)	De
PCNL							
exp. 1	134	1.25	0.37	0.56	1282	809	1.6
exp. 2	89	2.45	0.31	0.47	694	426	1.6
PLA control							
exp. 1	121	1.87	1.05	0.38	877	222	4.0
exp. 2	157	1.12	0.98	0.50	1515	419	3.6
PLA 4032D							
exp. 1	145	1.09	1.55	0.41	1515	226	6.7
exp. 2	125	1.61	1.10	0.54	1042	237	4.4

Figure 10 shows this data for both the PLA graft (PCNL) and homopolymer (PLA 4032D). Interestingly, the PCNL is almost completely linear during the entire experiment (Figure 10a), which compares well with the calculated Deborah number (1.6 in Table 2). In contrast, a lag in the polymer response was observed for the PLA homopolymer (Figure 10b,c), which also corroborates with the higher Deborah number (see Table 2). Therefore, in addition to diffusivities and relaxation time constants calculated from this diffusion-relaxation model, Figures 9 and 10 intuitively confirm the differences in water diffusivity and the relationship between water diffusion and polymer relaxation.

In addition to time-resolved FTIR-ATR spectroscopy experiments, gravimetric experiments were also conducted on PCNL, PLA control, and PLA 4032D. Figure 11 shows one of the experiments for PLA 4032D. This experiment was repeated for each polymer at least 5 times.

Although the Fickian model appears to adequately describe the liquid water sorption kinetics, the inset in the graph, which highlights the early time data, illustrates the difficulties in obtaining accurate dynamic sorption data with liquid diffusants using gravimetry. Unlike vapor gravimetry, liquid gravimetric experiments require manually removing the sample from the

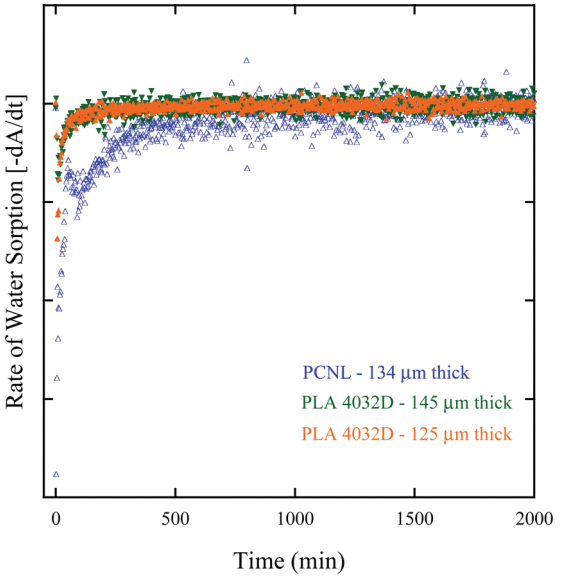

Figure 9. Rate of water sorption (derivative of time-resolved water H−O−H bending infrared absorbance data) versus time in PCNL (134 μm film thickness; blue triangles) and PLA 4032D (145 and 125 μm film thicknesses; green and orange triangles, respectively) at 25 °C.

liquid, blotting the surface free of surface liquid, quickly weighing on a balance and then reimmersing the film in the liquid. This is repeated many times over a short time interval to collect early time kinetic data. Unlike the in situ time-resolved FTIR-ATR spectroscopy technique, this ex situ technique introduces significantly larger error when attempting to collect many data points over a short time frame. Consequently, the regression error between the Fickian model and experimental data was many orders of magnitude higher in the dynamic gravimetric experiments compared to the FTIR-ATR experiment (see Table 3). In the FTIR-ATR experiments, the percent error between data and model was lower than the standard deviation between

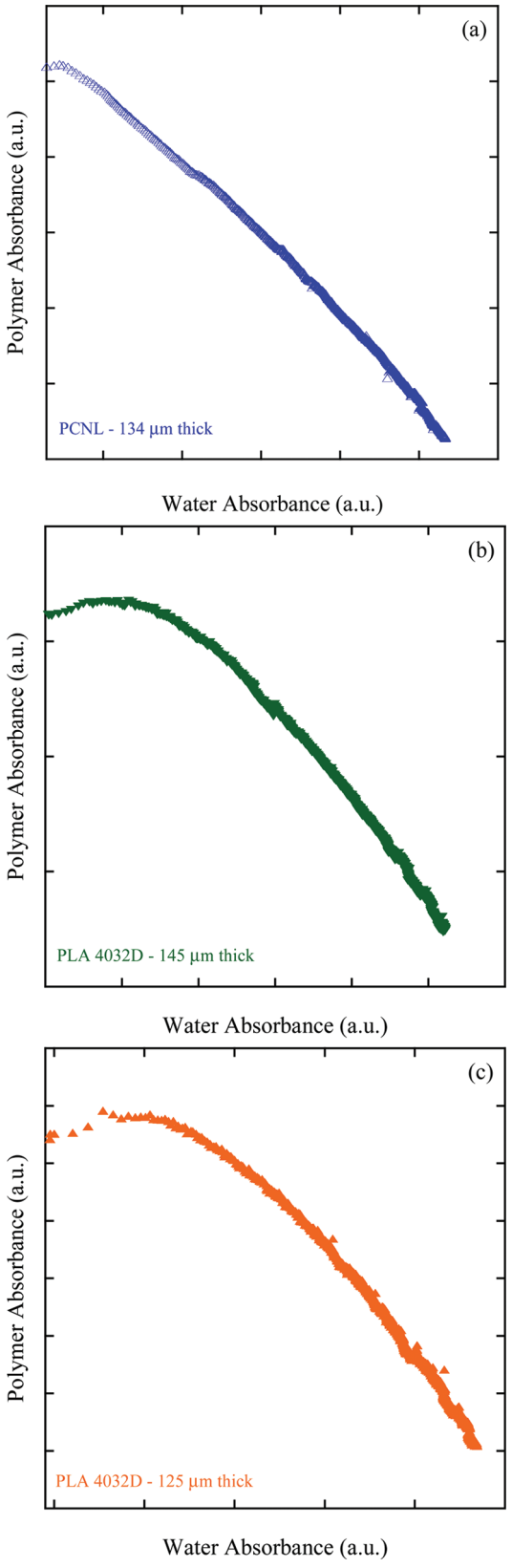

Figure 10. Polymer strain (time-resolved CH_3 bending infrared absorbance) versus water diffusion (time-resolved H−O−H bending infrared absorbance) at 25 °C for (a) PCNL (134 μm film thickness; blue triangles) and (b) PLA 4032D (145 μm film thickness; green triangles), (c) (125 μm film thickness; orange triangles).

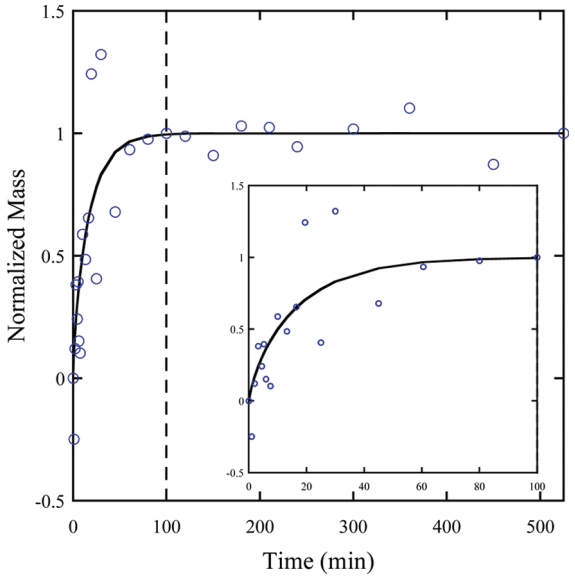

Figure 11. Liquid water sorption kinetics (gravimetry) in PLA 4032D film at ~25 °C. Solid line represents a regression to the Fickian model (eq 1). The inset is a magnified view of the early time data; first 100 min.

experiments (between exp. 1 and exp. 2 in Table 2). This was not the case for the dynamic gravimetric experiments. The regressed diffusivities from dynamic gravimetry were on the order of 1×10^{-8} cm^2/s for all films, but the regression error between model and data was too high to confidently report accurate values. However, the measured diffusivities from this technique were on the same order of magnitude as the diffusivities determined from FTIR-ATR spectroscopy.

Sharp et al.[8] also conducted dynamic gravimetric experiments of liquid water in PLA; the only other report on this in the literature to the authors' knowledge. They calculated diffusivity for liquid water in thicker, heavier PLA films than the ones reported in this study (over an order of magnitude thicker and heavier). Few data points were reported in the transient portion of the experiment; however, their data appear to be more accurate as one would expect with thicker, heavier films. However, for our study, the use of thicker films would result in experiments that are not comparable in thickness to the ATR experiments, where thicker films in ATR experiments would require extremely long times to adequately measure the relaxation phenomena. Additionally, heavier (thicker) films were not practical due to the sample size limitations of investigating newly synthesized polymers (e.g., PCNL). Interestingly, Sharp et al.[8] observed relaxation phenomena in their experiments when using a quartz spring microbalance to measure the sorption dynamics of water vapor in PLA; an experiment that is more sensitive than standard gravimetry.

It is important to note that the data from dynamic gravimetry appears Fickian, whereas the data collected from time-resolved FTIR-ATR spectroscopy reveals anomalous behavior. The higher error and lower sensitivity of gravimetry may be one reason for the inability to capture this anomalous behavior. Recently, Guo and Barbari[42] observed differences in dynamics between time-resolved FTIR-ATR (anomalous) and gravimetric sorption (Fickian) in their study on the sorption of acetonitrile vapor in glassy cellulose acetate. They attribute these differences to the more reliable early time data and the location specific absorbance

Table 3. Regression Error Analysis for Time-Resolved FTIR-ATR Spectroscopy and Dynamic Gravimetry Experiments in PCNL, PLA control, and PLA 4032D

sample	FTIR-ATR relaxation model SSE[a] × 10^4	FTIR-ATR diffusion-relaxation model SSE[a] × 10^4	dynamic gravimetry Fickian model SSE[a] × 10^4
PCNL	1.29 ± 0.80	6.44 ± 2.10	527 ± 377
PLA control	0.92 ± 0.52	4.66 ± 0.84	554 ± 347
PLA 4032 D	0.02 ± 0.02	5.84 ± 2.32	400 ± 141

[a] Sum of the squared error between model and data normalized by number of data points; values correspond to average and standard deviation from multiple experiments.

Table 4. Liquid Water Equilibrium Solubility in PCNL, PLA Control, and PLA 4032D

sample	$S \times 10^3$ (g_w/g_p)
PCNL	11.5 ± 2.1
PLA control	12.8 ± 3.1
PLA 4032 D	8.7 ± 1.2

(concentration) obtained with time-resolved FTIR-ATR spectroscopy. Therefore, the location specific, high sensitivity, and molecular-level resolution of time-resolved FTIR-ATR spectroscopy allows for the capability to identify changes in the local environment of both the diffusant and polymer; phenomena that are undetectable with gravimetric techniques. Also, one should note that there might be slight differences associated with free-standing films used in gravimetric techniques compared to constrained films used in FTIR-ATR spectroscopy. However, no measured differences have yet to be documented.

In contrast to the dynamic values obtained from gravimetric experiments, the equilibrium values that were obtained in this study were not as time sensitive and more weight measurements could be collected over a longer time period (see data >100 min in Figure 11). Therefore, the error was reduced by an order of magnitude compared to the dynamic portion of the experiments. Table 4 lists the equilibrium liquid water solubility for each film studied, where the values reported are the average and standard deviation of at least 5 experiments on each film. On average, the standard deviation for this experiment was ~25%, and the error associated with the balance was on average ~5%, calculated by comparing the accuracy of the balance with the change in mass recorded in the films (water gain). The PLA graft and hompolymers appear to all have a similar solubility. Although there are several studies that report water vapor solubility in PLA, few have reported on liquid water solubility. Sharp et al.[8] reported liquid water equilibrium solubility in PLA of 1.4% at 20 °C, which appears to fall within the range of the values reported here. These results suggest that PLA graft copolymers may enhance the barrier properties of PLA, where the water flux is reduced by a lower diffusivity in the polymer.

CONCLUSIONS

Time-resolved FTIR-ATR spectroscopy provides an accurate measurement of liquid water sorption kinetics in nonequilibrium glassy polymers (PLA homo and graft copolymers). Also, unlike gravimetric techniques, the FTIR-ATR technique captures multiple dynamic phenomena (diffusion and polymer relaxation) with molecular-level resolution. The non-Fickian behavior observed in this study, which was due to water diffusion and water-induced polymer relaxation occurring on the same time scale, was quantified and modeled. The calculated water diffusivity and rate of water sorption was significantly slower for the PLA graft copolymer (with only 5 wt % rubber) compared to the PLA homopolymer. These results suggest that the graft copolymer chain architecture not only substantially improves toughness but also results in improved barrier properties.

ASSOCIATED CONTENT

Supporting Information. Additional data including DSC thermograms of all polymer samples (PDF). This material is available free of charge via the Internet at http://pubs.acs.org.

AUTHOR INFORMATION

Corresponding Author
*E-mail: elabd@drexel.edu.

ACKNOWLEDGMENT

The authors acknowledge the financial support of the National Science Foundation (CBET-0644593) and the United States Department of Agriculture and the United States Department of Energy (06GO96002).

REFERENCES

(1) Auras, R.; Harte, B.; Selke, S. *Macromol. Biosci.* **2004**, *4*, 835–864.
(2) Sinclair, R. G. *J. Macromol. Sci., Part A: Pure Appl. Chem.* **1996**, *A33*, 585–597.
(3) Williams, C. K.; Hillmyer, M. A. *Polym. Rev.* **2008**, *48*, 1–10.
(4) Oliveira, N. S.; Gonçalves, C. M.; Coutinho, J. A. P.; Ferreira, A.; Dorgan, J.; Marrucho, I. M. *Fluid Phase Equilib.* **2006**, *250*, 116–124.
(5) Siparsky, G. L.; Voorhees, K. J.; Dorgan, J. R.; Schilling, K. *J. Environ. Polym. Degrad.* **1997**, *5*, 125–136.
(6) Li, G.; Li, H.; Turng, L. S.; Gong, S.; Zhang, C. *Fluid Phase Equilib.* **2006**, *246*, 158–166.
(7) Cairncross, R. A.; Ramaswamy, S.; O'Connor, R. *Int. Polym. Process* **2007**, *22*, 33–37.
(8) Sharp, J. S.; Forrest, J. A.; Jones, R. A. L. *Macromolecules* **2001**, *34*, 8752–8760.
(9) Elabd, Y. A.; Baschetti, M. G.; Barbari, T. A. *J. Polym. Sci., Part B: Polym. Phys.* **2003**, *41*, 2794–2807.
(10) Elabd, Y. A.; Barbari, T. A. *Polym. AIChE J.* **2002**, *48* (8), 1610–1620.
(11) Hallinan, D. T., Jr.; Elabd, Y. A. *J. Phys. Chem. B* **2007**, *111*, 13221–13230.
(12) Hallinan, D. T., Jr.; De Angelis, M. G.; Baschetti, M. G.; Sarti, G. C.; Elabd, Y. A. *Macromolecules* **2010**, *43*, 4667–4678.
(13) Elabd, Y. A.; Barbari, T. A. *AIChE J.* **2001**, *47* (6), 1255–1262.
(14) Theryo, G.; Jing, F.; Pitet, L. M.; Hillmyer, M. A. *Macromolecules* **2010**, *43*, 7394–7397.
(15) Iotti, M.; Fabbri, P.; Messori, M.; Pilati, F.; Fava, P. *J. Polym. Environ.* **2009**, *17*, 10–19.
(16) Chaiwong, C.; Rachtanapun, P.; Wongchaiya, P.; Auras, R.; Boonyawan, D. *Surf. Coat. Technol.* **2010**, *204*, 2933–2939.
(17) Chang, J. H.; An, Y. U.; Sur, G. S. *J. Polym. Sci., Part B: Polym. Phys.* **2003**, *41*, 94–103.
(18) Sanchez-Garcia, M. D.; Gimenez, E.; Lagaron, J. M. *Carbohydr. Polym.* **2008**, *71*, 235–244.
(19) Gorrasi, G.; Vittoria, V.; Murariu, M.; Da Silva Ferreira, A.; Alexandre, M.; Dubois, P. *Biomacromolecules* **2008**, *9*, 984–990.

(20) Berens, A. R.; Hopfenberg, H. B. *Polymer* **1978**, *19*, 489–496.
(21) Auras, R.; Lim, L. T.; Selke, S. E. M.; Tsuji, H., Eds. *Poly(lactic acid): Synthesis, Structures, Properties, Progressing, and Application*; Wiley: New York, 2010.
(22) Crank, J. *Mathematics of Diffusion*, 2nd ed.; Wiley: New York, 1975.
(23) Hallinan, D. T., Jr.; Elabd, Y. A. *J. Phys. Chem. B* **2009**, *113*, 4257–4266.
(24) Meaurio, E.; Lopez-Rodriguez, N.; Sarasua, J. R. *Macromolecules* **2006**, *39*, 9291–9301.
(25) Zhang, J.; Tsuji, H.; Noda, I.; Ozaki, Y. *Macromolecules* **2004**, *37*, 6433–6439.
(26) Zhang, J.; Tsuji, H.; Noda, I.; Ozaki, Y. *J. Phys. Chem. B* **2004**, *108*, 11514–11520.
(27) Garlotta, D. J. *Polym. Environ.* **2001**, *9*, 63–84.
(28) Sarasua, J. R.; Lopez-Rodriguez, N.; Arraiza, A. L.; Meaurio, E. *Macromolecules* **2005**, *38*, 8362–8371.
(29) Zhang, J.; Duan, Y.; Sato, H.; Tsuji, H.; Noda, I.; Yan, S.; Ozaki, Y. *Macromolecules* **2005**, *38*, 8012–8021.
(30) Kister, G.; Cassanas, G.; Vert, M. *Polymer* **1998**, *39*, 267–273.
(31) Urayama, H.; Moon, S. I.; Kimura, Y. *Macromol. Mater. Eng.* **2003**, *288*, 137–143.
(32) Bourque, H.; Laurin, I.; Pézolet, M. *Langmuir* **2001**, *17*, 5842–5849.
(33) Klass, J. M.; Lennox, R. B.; Brown, G. R.; Bourque, H.; Pézolet, M. *Langmuir* **2003**, *19*, 333–340.
(34) Proikakis, C. S.; Mamouzelos, N. J.; Tarantili, P. a.; Andreopoulos, A. G. *J. Appl. Polym. Sci.* **2003**, *87*, 795–804.
(35) Gordon, S. H.; Cao, X.; Mohamed, A.; Willett, J. L. *J. Appl. Polym. Sci.* **2005**, *97*, 813–821.
(36) Braun, B.; Dorgan, J. R.; Dec, S. F. *Macromolecules* **2006**, *39*, 9302–9310.
(37) Tretinnikov, O. N.; Kato, K.; Iwata, H. *Langmuir* **2004**, *20*, 6748–6753.
(38) Fukushima, K.; Kimura, Y. *Polym. Int.* **2006**, *55*, 626–642.
(39) Barrer, R. M. Diffusion and Permeation in Heterogeneous Media. In *Diffusion in Polymers*; Crank, J., Park, G. S., Eds.; Academic Press: London, 1968; pp 165−217.
(40) Frisch, H. L. *Polym. Eng. Sci.* **1980**, *20*, 2–13.
(41) Vrentas, J. S.; Jarzebski, C. M.; Duda, J. L. *AIChE J.* **1975**, *21*, 894–901.
(42) Guo, J.; Barbari, T. A. *Macromolecules* **2009**, *42*, 5700–5708.